IEEE Access
Multidisciplinary | Rapid Review | Open Access Journal

Received April 10, 2019, accepted April 23, 2019, date of publication April 29, 2019, date of current version May 9, 2019.

Digital Object Identifier 10.1109/ACCESS.2019.2913474

The Effects of Walking Speed and Hardness of Terrain on the Foot-Terrain Interaction and Driving Torque for Planar Human Walking

CHUANXIAO YANG[1], LIANG DING[1], (Senior Member, IEEE), KUNPENG WANG[2], RONG SONG[3], (Member, IEEE), DEWEI TANG[1], HAIBO GAO[1], AND ZONGQUAN DENG[1]

[1]State Key Laboratory of Robotics and Systems, Harbin Institute of Technology, Harbin 150080, China
[2]China Academy of Aerospace Aerodynamics, CH UAV Technology Co., Ltd., Shenzhen, China
[3]School of Biomedical Engineering, Sun Yat-sen University, Shenzhen 510006, China

Corresponding authors: Liang Ding (liangding@hit.edu.cn) and Dewei Tang (dwtang@hit.edu.cn)

This work was supported in part by the National Natural Science Foundation of China under Grant 51575120, in part by the Outstanding Youth Foundation under Grant 51822502, in part by the Foundation for Innovative Research Groups, National Natural Science Foundation of China, under Grant 51521003, in part by the Foundation of the Chinese State Key Laboratory of Robotics and Systems under Grant SKLRS201501B and Grant SKLRS20164B, in part by the Application and Development Program of Harbin under Grant 2015RQQXJ081, and in part by the 111 Project under Grant B07018.

ABSTRACT The foot-terrain interaction mechanics of human is important in understanding the biped locomotion mechanism. This paper aims to investigate the effect of walking speed and the hardness of the terrain on foot-terrain interaction mechanics. In the experiments, mobile portable plantar mechanical measuring insoles with 107 sensor elements were used to gauge the plantar force and contact area in real-time. Seven subjects with healthy feet have participated in typical experiments. The statistical methods including correlation analysis, univariance analysis, and systematic identification are primarily used to obtain several main results. Bimodal functions in describing the total pressure-time relations were performed at slow and regular speeds but only one hump is left if walking at fast paces; they can be unified and summed by three subsections' unimodal functions. The forefoot produces a large peak impact force in slow and regular quasi-static walking on both hard ground and deformable terrains, while the heel absorbs more dynamic impact shocks in fast walking on hard ground. The torques generated by the ankle joints are calculated based on plantar force or its derived information such as zero moment point. Some implications are drawn, for example, the dynamically changed positions of zero moment point (ZMP) for humans are similar to that generated by reptiles wiggling through the flowable terrains; increasing the stride length on the hard ground produces more impact vibrations than quickening paces but more effective in accelerating walks on deformable terrains.

INDEX TERMS Foot-terrain interaction mechanics of human, plantar force, walking speed, deformable terrain, unimodal functions, ankle torque.

I. INTRODUCTION

The biped walking mechanism has attracted enormous interests from communities of both the humanoid robotic research [1]–[3] and medical science in terms of assisted rehabilitation therapy of diabetic foot [4]–[6]. The feet, as the moving structure in humanoid robots or evolved appendage [7] in human body, play a significant role in supporting the upper body through direct interacting with the terrain surface. More substantially, the foot-terrain interaction mechanics are essential in predicting contact forces and simulating kinematic performance for legged robot, but still at its budding stage. Considering the influential factors, the foot-terrain interaction is primarily affected by the motion parameters which are mainly referred to the walking speed for human, terrain properties, as well as other less prominent factors such as the dynamics of arc system, properties of the soft tissue, and even the shod foot structure.

There are many qualitative descriptions of the influences of walking speed on human foot-terrain interaction mechanics.

The associate editor coordinating the review of this manuscript and approving it for publication was Neil Yuwen Yen.

Recent studies have provided new evidence that increasing walking speed resulted in a significantly higher peak plantar heel pressure [8]–[11], even wearing the high-heeled shoes [12]. In these researches, different burdens and distributions of plantar pressures with relevance to the weight, height, and foot dimensions [13]–[15] are considered as the contributors to the foot-terrain interaction mechanics for diverse subjects, even associated with shoe stiffness and dynamic response. The stance during one stride cycle for human walking includes four step phases, called the loading response (LR), midstance (MS), terminal stance (TS), and pre-swing (PS) phases, respectively [16]. Each during time is relative to the heel impulse and lift force due to the leverage effect. However, most of these researches were conducted on-treadmill ambulation [17], on which the stance period can be shortened as much as 6.7% at an identical speed with that on rigid ground [18], leading to a more dynamically changed plantar force. Therefore, the properties of plantar force on treadmills are distinguished from that on natural ground.

The influences of terrain rigidity to foot-terrain interaction have been focused in the field of legged robotics. For rigid terrain, to bridge between the contact force and motion parameters, multi-rigid-chain contact models [19], describing the constraints in kinematics, and elasto-plastic models [20], capturing the combination effects of transient and permanent deformations generated by contact bodies on contact mechanics [21], [22] have been applied to the field of legged robotics. A simple spring-mass is sufficient in describing the interdependence and magnitudes of these major mechanical properties for running and hopping animals on rigid ground [23]. Furthermore, a versatile volumetric deformation-based model was proposed with point-like elements and superellipsoid-plane assumptions [24]. However, precedent forward dynamic simulations on biped walking performance [24], [25] rarely considered the distribution of plantar pressures and deformations on terrain surface in details, while a point-like contact occurring at the foothold is often hypothesized [25]. As remedies, additional damping terms are added for these models in forward and reverse dynamic simulations during human walking on deformable surfaces with even flowability and slippage [14]. To reduce the rigid collision but increase the damping, the robotic feet are often wrapped by rubber pad at the bottom [26]. Differing from rigid ground walking, a semi-empirical approach in the subject of terramechanics, revealing the principles of contact mechanics between off-road locomotors and deformable terrains is available [27], [28]. These models based the resistive force theory can also be used to predict the penetration forces between intrusion locomotors and the fluidized granular substrates [7]. However, they were not widely used concerning on human walking occasions, this research will be of benefit to the bionic studies of legged robotics. The studies of human walking on naturally rigid ground and deformable terrains are still open issues.

Some other indirect factors also contribute to the foot-interaction mechanics. From studies on the samples extracted from cadaveric foot, the stiffness of soft tissue, as a factor affecting the foot-terrain interaction forces, will be enlarged as the loading frequency is increased [29], [30]. In practice, the measurement of contact forces between soft tissues and ground in situ test [31] is pursued due to its precise description on natural compact. However, the effect of soft tissue deformation is so small that can be neglect compared with that of terrain deformation in the off-road walking occasions. More practically, soft issues at heel pads interacting with rigid ground were often described by non-linear viscoelastic models [32]. The linkages among heel, phalangeal joint, and toe (can be approximated by three spheres [33]) will add viscosity and response delay for the total system. Furthermore, a scaling effect should be considered in mapping the relation of contact stiffness and damping of the underlying soft tissues of human feet [34] to robotic design. For high-heeled shod feet [35], the feet are much easier to be trapped into deformable terrains and heel-break is primarily caused by buckling failure on hard ground.

Most of the current researches conducted on the treadmill are beneficial to understanding the biped walking mechanism. However, the foot-terrain interaction mechanics have not been investigated if human is walking on natural terrain surface, including both rigid ground and soft terrains. Quantitative descriptions on speed-dependent modeling of interaction mechanics for human walking on natural terrains were also rarely studied. Therefore, the influences of natural terrain with different rigidities and walking speeds on foot-terrain interaction mechanics should be carried out, which will contribute to the fields of both human and humanoid robotic research.

The main contributions of this paper lie in: 1) quantitatively and qualitatively descriptions on contact mechanics of forefoot, middle foot, and heel for biped walking on natural terrains; 2) investigation of influence of the speed and terrain rigidity on the foot-terrain interaction forces and driving ankle torques; 3) study of a hybrid model including spring-dashpot functions and simplified inverse dynamics, considering some indirect information including the step length, stride frequency, ZMP (zero moment point), and energy.

II. METHOD

In this research, the medilogic telemetric system with the hardware (two modems with specified batteries and test sensors) and software manufactured by the T&T medilogic Medizintechnik Co., Ltd were used to measure the plantar normal force for human. The leathered insole is categorized into 107 sensor elements on entire plantar area (in which 46 sensor elements are used to measure the forefoot pressures, 30 elements to measure the midfoot pressures, and 31 to measure the heel pressures, respectively).

A. EXPERIMENTAL APPARATUS

These measurement insoles were connected with a signal emission device tied around the subject's waist. A second

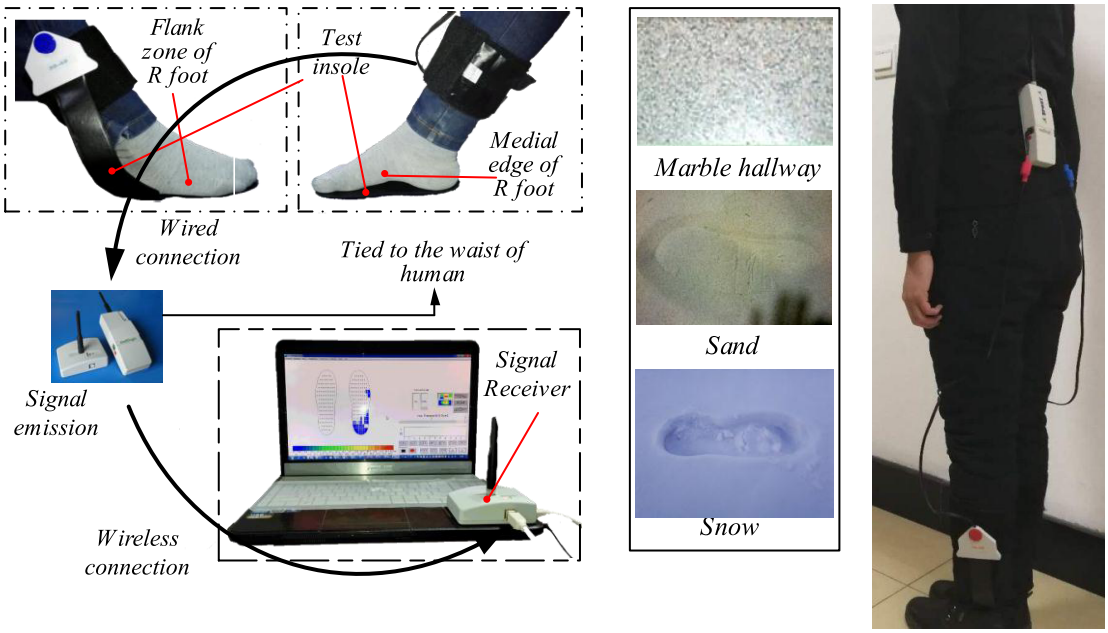

FIGURE 1. Gauging platform of the plantar pressure testbed, of which the hardware in gauging platform includes the test insoles with signal acceptor and emission device, while the software that recording the experimental data.

modem attached directly to the USB-port of a computer measured data and transmitted them through a cable. The experimental study on human foot-terrain interaction forces has been conducted in two groups: one is the steady level walking on rigid terrain paved by ground tile at different walking speeds and the other is on two deformable natural terrains (snow and sand) at perceived comfortable speed. The snow was naturally accumulated on the top of an even concrete roof, thus the surface of the snow is smooth with an average depth of approximately 130.0mm. The sand particles were laid in a big soil bin and they were smoothed by a mechanical scraper after each test, and the depth of the sand was made to be the same as that of the snow. T&T Medilogic data acquisition and processing system was used to measure the plantar normal forces in real time. The insoles were placed between the wearing shoes and feet in socks, of which the deformation was adjusted by the reserved space. The sampling frequency was set to 60 Hz and the time interval was chosen to be 0.0167s. Furthermore, the experimental data depicted in figures can be easily extracted and filtered. By referring to other relative researches [5], [11], the participants in our experiments are 7 healthy adults from 23 to 29 years old with the weight ranging from 62.2kg to 80.2kg. The height is from 1.71m to 1.80m and their biological foot structures are regular. All the seven adults have participated in the typical experiments on hard ground while two subjects of them have participated in the typical experiments on soft terrains, in which we find the contours of the force-time curves are similar to one another. We found their plantar forces are similar with each other and then we only chose one to represent others. The representative subject is 60.8kg weight, 25 years old, and 1.74m tall (plantar area of forefoot: 7223mm^2; midfoot: 4645mm^2; heel: 4813mm^2). The power supply unit (24V 2A) was provided and sufficiently charged. More details of the measurement apparatus have been illustrated in Fig. (1).

TABLE 1. Desired speed groups and their measured values in reality (m/s).

Desired walking speeds	1.10	1.32	1.54	1.76	1.98	2.20
Measured walking speeds	1.11	1.36	1.49	1.76	1.95	2.19

Generally, the walking speed of a human ranges from 4km/h to 8km/h (about 1.11 $\sim$ 2.22m/s). Thus, we set the slowest speed to be 1.10m/s and the fastest one to be 2.20m/s. Five equal intervals are separated into within the range from 1.10 to 2.20m/s and the desired speeds are shown in Table 1.

Three methods have been used to control the walking speeds. 1) An acceleration sensor was used, developed by LANCE technologies inc., to detect the temporal variation of speed, of which the magnitude is controlled to be zero as far as possible with an error smaller than 0.05m/s^2. 2) The walking experiments were conducted at a long distance of 15m with constant speed and the walking periods of each speed were controlled to achieve different walking speeds. 3) Several experiments were conducted for each speed and we chose the steadiest results corresponding to constant speeds. Thus, the average walking speed is achieved by: $v = S/\Delta t$. The measured values in reality are listed in Table 1.

B. ANALYSIS OF THE EXPERIMENTAL DATA

Three types of software are employed in this study, including the Medilogic software, Microsoft Excel, and Matlab. The data collected by the Medilogic software are in the format of CSV (Comma-Separated Values), which can be directly imported into Excel and be dealt with GUI (Graphical User Interface) program in Matlab. The statistical methods including correlation analysis, multivariable analysis, and systematic identification have been used to analyze the experimental data.

The Fourier equations were used to establish the force-time relations of different subsections. Moreover, the normal impulses generated by three subsection forces and stresses are analyzed based on the establishment of Fourier fitting functions. The fits qualities of such approach can be assured that larger than 96% at four levels:

$$F_{\text{sub}i} = a_0 + \sum_{j=1}^{4} [a_j \cos(j\omega t) + b_j \sin(j\omega t)] \tag{1}$$

where $F_{\text{sub}i}$ ($i = 1 \sim 3$) is the plantar force generated by the forefoot, midfoot, and heel, respectively; a_j, b_j, are the fitting Fourier coefficients. Eqn. (1) is an unimodal function while their asynchronous overlap, expressed in Eqn. (2) may be not, whereas the total plantar force $F(t)$ exhibits multiple poles. The unimodal function indicates the walk is governed by only one group of compression and restitution stages.

$$F(t) = \sum_{i=1}^{3} F_{\text{sub}i}(t) \tag{2}$$

According to the energy law, the dynamic impact absorbed by the heel impact, represented by I_h, is positively associated with the kinetic energy.

$$I_h = \frac{1}{2}[\int_{t_{hc}}^{t_{hc}+0.5T} F_{\text{sub}3}(t)dt]^2 \tag{3}$$

In regular walking, the force-time relation consisting of four intervals can be observed, characterized as four phases. Focusing on the average force change rates $\mathrm{d}F/\mathrm{d}t$ ($i = 1 \sim 4$) at the 1st to 4th phases, and three extreme values - two peak and one minimal values, these seven parameters $P_i(v, t)$ ($i = 1 \sim 7$) on plantar pressure master curves were defined and their variations at different walking speeds were estimated. The relations between each parameter, represented by P_i, and walking speed v can be revealed by a linear fitting function. The slopes of each linear function are indicated by ζ_i (v) ($i = 1 \sim 7$). It is theoretically defined as the derivatives of average force change rates at four contact phases and three extreme values to the walking speed. We hypothesize that:

$$P_i(v) = \zeta_i \cdot v + C_i \tag{4a}$$

$$\frac{dp_i(v)}{dv} = \zeta_i(v, t) = \begin{cases} \dfrac{dF_{pi}^2(v)}{\partial^2 v} \\ \dfrac{dF_{ext(i-4)}(v)}{dv} \end{cases} \tag{4b}$$

where F_{pi} ($i = 1 \sim 4$) is the functions of contact forces at four phases, $F_{\text{ext}i}$ ($i = 1 \sim 3$) denotes the three extreme values in force functions, $C_i (i = 1 \sim 7)$ are the constants in fitting linear functions, respectively. It was found the force change rates at phase 1 (P_1), phase 2 (P_2), and the peak value 1 (P_5) tend to increase with the acceleration was executed. However, the force change rate at phase 3 (P_3), phase 4 (P_4), the 2nd peak value (P_6), and minimal value (P_7) had the opposite trend. Concerning on the goodness of fit in function of Eqn. (1), defined by Eqn. (5) and represented by R_i, larger magnitude of R_i indicates the higher linear relation between the average walking speed v and prescribed seven parameters.

$$R_i = 1 - \left(\frac{\sum_{j=1}^{m} \left| P_i(v_j) - P_{\exp i}(v_j) \right|}{\sum_{j=1}^{m} \left| P_{\exp i}(v_j) \right|} \right)^2 \tag{5}$$

where $P_i(v_j)$ denotes the i-th parameter and j-th sampling point of walking speed; $P_{\exp i}(v_j)$ is the corresponding experimental data, m is the total sampling number.

C. DERIVATION OF ZERO MOMENT POINT BASED ON PLANTAR FORCE

The step length l_y along the y-direction during one single stride can be obtained by: $l_y = 0.5vT$, T denotes the period of cycle. The origin was set to bottom left corner of the left heel, ZMP (zero moment point) indicating the point where resultant moment from each contact pressure is zero, during one typical cycle can be calculated as:

If $t \in (t_{p1}, t_{hc} + 0.5T]$

$$\begin{cases} x_{zmp} = x_0 \\ y_{zmp} = \dfrac{F_{sub3}(t) \cdot d_h + F_{sub2}(t) \cdot d_m + F_{sub1}(t) \cdot d_f}{\sum_{i=1}^{3} F_{subi}(t)} \end{cases} \tag{6a}$$

If $t \in (t_{hc} + 0.5T, t_{p1} + 0.5T]$

$$\begin{cases} x_{zmp} = \dfrac{\sum_{i=1}^{3} F_{subi}(t + 0.5T) \cdot (x_0 + l_x) + \sum_{i=1}^{3} F_{subi}(t) \cdot x_0}{\sum_{i=1}^{3} F_{subi}(t + 0.5T) + \sum_{i=1}^{3} F_{subi}(t)} \\ y_{zmp} = \dfrac{\sum_{i=1}^{3} \{[F_{subi}(t + 0.5T) + F_{subi}(t)] \cdot d_{subi}\}}{\sum_{i=1}^{3} F_{subi}(t + 0.5T) + \sum_{i=1}^{3} F_{subi}(t)} \\ \qquad + \dfrac{l_y \cdot \sum_{i=1}^{3} F_{subi}(t + 0.5T)}{\sum_{i=1}^{3} F_{subi}(t + 0.5T) + \sum_{i=1}^{3} F_{subi}(t)} \end{cases} \tag{6b}$$

where t_{p1}, t_{hc} are the time when the first peak value and heel contact occur respectively; x_{zmp}, y_{zmp} are the positions of ZMP along the width (x axis) and length (y axis) directions of the foot, respectively; x_0 denotes the x position of pressure center (the x positions of heel, midfoot, and forefoot pressures were pretty close to each other); $d_{\text{sub}i}$ ($i = 1 \sim 3$) represent the y positions of heel, midfoot, and forefoot pressures; T, l_x, l_y denotes the period of cycle, the distance between left and right feet along x axis, and step length along y axis. It notes that the single support phase happened at the time interval $(t_{\text{p1}}+0.5nT, t_{\text{hc}}+0.5nT]$ or $(t_{\text{p1}}+0.5nT, t_{\text{hc}}+0.5\text{n(T}+1)]$, and the DSP (double support phase) was indicated by the time interval $(t_{\text{hc}}+0.5\,nT, t_{\text{p1}}+0.5n(T+1)]$ or $(t_{\text{hc}}+0.5\,nT, t_{\text{p1}}+0.5nT](n = 1, 2, 3\cdots)$. When one foot is stepping on the ground, the position of ZMP lies within the scope of the specified foot; however, if both of the two feet step on the ground, the position of ZMP will be located at a middle area between them. Consequently, the trajectories of ZMP, i.e., the dynamically changed position of ZMP for both single and double support phases, can be calculated by Eqn. (6).

D. DERIVATION OF DRIVING ANKLE TORQUE BASED ON ZERO MOMENT POINT

Based on dynamics of multi-rigid chains, the dynamics for the stance foot at single support phase can be expressed as:

$$\begin{aligned}\boldsymbol{M}_T + \boldsymbol{OP}_{\text{zmp}} \times \boldsymbol{F} + \boldsymbol{OG}_f \times m_f\boldsymbol{g} - \boldsymbol{M}_a - \boldsymbol{OO}_a \times \boldsymbol{F}_a \\ = \sum \dot{\boldsymbol{A}}_f + \sum \boldsymbol{OG}_f \times m_f\boldsymbol{a}_f \end{aligned} \tag{7}$$

where $\boldsymbol{M}_{\text{T}}$ and $\boldsymbol{M}_{\text{a}}$ denote the moments generated by tangential force in action on the origin O (any position) and the rest of body that exclusive of stance foot exerted on the ankle; $\boldsymbol{OP}_{\text{zmp}}$, $\boldsymbol{OO}_{\text{a}}$ are the ZMP (zero moment point) and ankle position vector in three dimensions; $\boldsymbol{F}$, $\boldsymbol{F}_{\text{a}}$ reveal the plantar force and external forces by the rest of body on the ankle; m_{f}, $\boldsymbol{a}_{\text{f}}$, and $\boldsymbol{G}_{\text{f}}$ indicate the gravity, linear acceleration and position of the center of foot; $\boldsymbol{A}_{\text{f}}$ is the angular acceleration in action on $\boldsymbol{G}_{\text{f}}$. If the origin O is set on contact surface, $\boldsymbol{M}_{\text{T}}$ can be neglected. Hence, if O is set on the ZMP point P_{zmp}, Eqn. (7) can be simplified into the following expression [36]:

$$\boldsymbol{M} = \boldsymbol{M}_a + \boldsymbol{P}_{\text{zmp}}\boldsymbol{O}_a \times \boldsymbol{F}_a = \boldsymbol{P}_{\text{zmp}}\boldsymbol{G}_f \times m_f\boldsymbol{g} \tag{8}$$

where $\boldsymbol{M}$ is the terminal output of eccentric bending moment exerted on the foot rotation axis, or the ankle. Subsequently, the moment $\boldsymbol{M}$ can be easily obtained if the tangential force is ignored, with these inputs including zero moment point vector $\boldsymbol{P}_{\text{zmp}}$ in Eqn.(6) and feet gravity $\boldsymbol{G}_{\text{f}}$.

E. PLANTAR FORCE-DEFORMATION RELATION IN SPING-DASHPOT MODEL BASED ON PLANTAR FORCE

The constitution of foot can be revealed by the distribution of bearing forces, of which the profiled and top views are sketched in Fig. 2. The interaction begins with a heel-strike, which can be indicated by a sphere [33], on rigid terrain. Hertz model [20] with fewer parameters to be identified was often used. Without considering arc system, midfoot is a thin linkage that transforming the pressure from heel to forefoot and produces a resisting torque to retard strike. A web-shaped force area can be observed in forefoot subsection in Fig. 2 (c), which enlarges contact area and prevents the body laterally tumbling. The entire foot system can be regarded as arc-type skeletal structure [37] while walking is implemented by a leverage lifting process [38]. At initial time, the foot hit the ground by only the heel-strike with the terrain surface, in which the deformation of sphere is enlarged, as shown in Fig. 2 (a). The plantar contact area is dominated by the heel and the variations in mechanical properties are captured by the 1st phase and 1st peak force. At this phase, the total plantar pressure will exceed the human weight, of which an extra part is produced in resisting the inertial force, until the maximum deformation of heel represented by a sphere is obtained; as the total plantar area impacts on the ground surface, the heel, midfoot, and forefoot all bear the upper load. Then, the deformation sets out to recovery, suggesting the contact force generated by heel gradually gets smaller. At about first half of the 2nd phase, the midfoot just contacts with the terrain and its deformation is gradually enlarged. However, in spite of the tiny effects of fascia [39] on mechanics, the midfoot as well as the heel leave the terrain nearly simultaneously and restitute to their free status. At this phase, the subject attempts to lift the heel about toe joints and the center of mass for human body has reached the lowest altitude during stride. A critical time that the total pressure equals body weight at the 2nd phase should be noticed, which is exactly the time when the peak value of midfoot pressure occurs. At 2nd half of the 2nd phase, when the sum of these three forces has dropped down to the value of human body weight, the work that resultant force of plantar forces and body gravity turns to be upward again; a large magnitude of energy is consumed by the ankle joint and forefoot due to the leverage effect of forefoot. This is the 3rd phase when both heel and forefoot pressures diminish, and the center of mass (COM) of human rises remarkably. Depending on structures of these connected phalanges, talus, calcaneus, the rotation moment maximizes and then decrease to let the body drop down. At this phase, the human body seems likely to function as an inverted pendulum in short period; because the toe-off phase has occurred and the heel of the other foot falls down, the upper loads are taken over by the other heel. Forefoot pressure under prescribed foot will be decreased to zero as revealed in 4th phase. However, the walking process for humanoid robots differ from that for human [40] considering various body structures, actuator types, transmissions, and even algorithms, which need a large temporal dynamic compensation.

From perspective of structure construction, the heels' resistance to impact is weakened dramatically in walking on deformable terrains such as sand and snow. Hence, they perform plasticity and fluidity, indicating that paddling or swimming is the major role that feet play. Thus the webbed, flattened, and fan shaped forefoot, a subsection that like ducks', is much capable of pushing these fluidized substrates, which can be significantly applicable in humanoid robotic

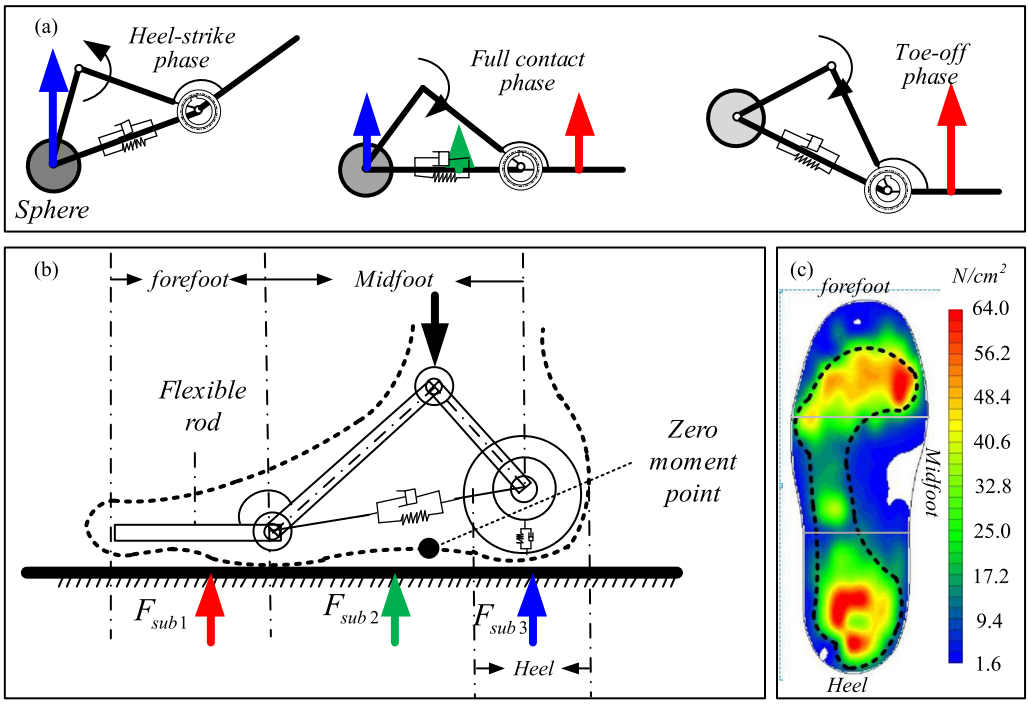

FIGURE 2. Schematic principles of (a) heel-strike, full contact, and toe-off phases; (b) simplified contact mechanism for three subsections in foot on planar in side view; as well as (c) the experimental image in top view. The heel interacting with the terrain can be approximated by a sphere, for which the indentation-force relation can be solved by Hertz constitutive model [36] (represented by a damping and spring system); the midfoot can be regarded as an arch-type skeletal structure [37]; the forefoot can be represented by a flexible rod connected to midfoot with a torsional spring based on leverage effect [38].

foot design. The shock-absorbing effects are not obvious for midfoot on deformable terrains. We can find little mechanical vibration are produced if humans walk on the rigid ground at a small magnitude of stride length or low frequency range, but leading to a slow walking in turn. Comparably, to accelerate paces for humanoid robots that walk on hard ground, enlarging the frequency is a more effective approach. However, increasing the stride length should also be focused if robots step on deformable terrains, like that the ostrich runs on the sand.

Regular biped walking is accommodated by adapting the stiffness of muscles and fascia to the walking speed and terrain conditions. Additionally, due to the fact that Hertz contact model doesn't consider the effect of damping term, Spring-dashpot model [26], [41] based on experimental data has been used to indicate the force-deflection relations. The 2nd and 3rd phases are contributed by compound effects of heel, midfoot, and forefoot interaction with the terrain. A right hand coordinate system in which the normal direction is along the leg and perpendicular to the ground at the contact point between heel/midfoot/forefoot and ground was fixed. Then the force-deformation relation between human feet and rigid terrain, using a spring-dashpot model [26], [41] based on non-linear constitutive relations, as well as the relation between rigid feet and deformable terrain based on terramechanics [28], are established respectively. We note that the feet deformation is in series with that on deformable terrain, only one model is enough in our descriptions. Since the spring-dashpot model is more widely applied, we use it to establish the compound effect for both deformations. If $\Delta z_{\mathrm{sub}i} > 0$:

$$F_{\mathrm{sub}i}(t) = K_i \Delta z_{\mathrm{sub}i}^{n_i}(t) + C_i \Delta z_{\mathrm{sub}i}^{p_i}(t) \left[\frac{d\,\Delta z_{\mathrm{sub}i}(t)}{dt} \right]^{q_i} \quad (9)$$

where $\Delta z_{\mathrm{sub}i}$ $(i = 1, 2, 3)$ represents the deformation on heel, midfoot, and forefoot at normal direction respectively; K_i and C_i indicate the contact normal stiffness and damping for these three subsections respectively; n_i, p_i, q_i are non-linear exponential terms. Five parameters remain to be identified in functions. Furthermore, these parameters in the heel, midfoot, forefoot contact models, including the stiffness K, damping coefficient C, and their nonlinear exponential terms n, p, q have been identified. Based on the referred literature [21] and our experimental data, the normal stress-strain relations of human feet and contact areas $A_{\mathrm{sub}i}(t)$ $(i = 1, 2, 3)$ on different subsections can both be obtained. The relations between normal pressures and deformations would be achieved through integration at the plantar area.

F. DRIVING ANKLE TORQUES BASED ON A SIMPLIFIED LOWER LIMB-FOOT SYSTEM

Considering the contact dynamics of biped locomotion on deformable terrain as illustrated in Fig.3 (a), we only care about the ankle joint that produced by tendons and

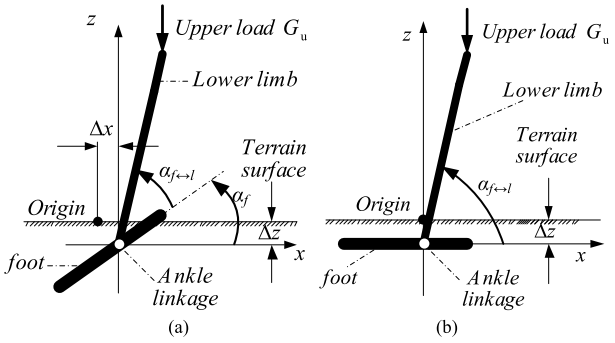

FIGURE 3. Schematic principles for a simplified lower limb-foot system while walking on deformable terrains (a) in general occasion and (b) vertical compaction.

muscles. Thus the body, upper limb, and lower limb overall are regarded as a unity, which is represented by the lower limb. In the side view, there are four displacements in general coordinate - Δx, Δz, α_{f}, $\alpha_{\mathrm{f}\leftrightarrow 1}$. Entire kinetic and potential energies are expressed as:

$$\sum E_k = \frac{1}{2}m_f(\Delta\dot{z}^2+\Delta\dot{x}^2)+\frac{1}{2}J_f\dot{\alpha}_f^2+\frac{1}{6}m_l(\xi_x+\xi_z) \quad (10a)$$

$$\sum P = m_f g\Delta z + m_l g[\Delta z + \frac{l_1}{2}\sin(\alpha_{f\leftrightarrow l}+\alpha_f)] \quad (10b)$$

where m_f and J_f denote the mass and rotary inertia of foot; ξ_x and ξ_y are intermediate variables that governed by:

$$\begin{aligned}\xi_X &= 3\Delta\dot{X}^2 - 3\Delta\dot{X}l_1(\dot{\alpha}_{f\leftrightarrow l1}+\dot{\alpha}_f)\sin(\alpha_{f\leftrightarrow l1}+\alpha_f)\\ &\quad + l_1^2(\dot{\alpha}_{f\leftrightarrow l1}+\dot{\alpha}_f)^2\sin^2(\alpha_{f\leftrightarrow l1}+\alpha_f) \quad (11a)\\ \xi_z &= 3\Delta\dot{z}^2 + 3\Delta\dot{z}l_1(\dot{\alpha}_{f\leftrightarrow l1}+\dot{\alpha}_f)\cos(\alpha_{f\leftrightarrow l1}+\alpha_f)\\ &\quad + l_1^2(\dot{\alpha}_{f\leftrightarrow l1}+\dot{\alpha}_f)^2\cos^2(\alpha_{f\leftrightarrow l1}+\alpha_f) \quad (11b)\end{aligned}$$

Here it is supposed that the center of mass of foot lies at the ankle linkage and that of the lower limb is on the middle point of its length l. m_l is its mass. We build the LaGrange functions based on inverse dynamics for multi-chains in form of matrix:

$$\begin{bmatrix}F_N-G_u\\F_T\\M_f\\M\end{bmatrix} = H_q\begin{bmatrix}\Delta\ddot{z}\\\Delta\ddot{x}\\\ddot{\alpha}_f\\\ddot{\alpha}_{f\leftrightarrow l}\end{bmatrix} + I_q\begin{bmatrix}\Delta\dot{z}^2\\\Delta\dot{x}^2\\\dot{\alpha}_f^2\\\dot{\alpha}_{f\leftrightarrow l}^2\end{bmatrix} + C_q\begin{bmatrix}\Delta\dot{z}\Delta\dot{x}\\\Delta\dot{z}\dot{\alpha}_f\\\Delta\dot{z}\dot{\alpha}_{f\leftrightarrow l}\\\Delta\dot{x}\dot{\alpha}_f\\\Delta\dot{x}\dot{\alpha}_{f\leftrightarrow l}\\\dot{\alpha}_f\dot{\alpha}_{f\leftrightarrow l}\end{bmatrix} + G_q \quad (12)$$

where F_{N}, $G_{\mathrm{u}}F_{\mathrm{T}}$, and M_{f} are the foot-terrain contact normal force, bearing upper load from upper body, tangential force and ankle moment, respectively. These inertial matrixes H_q, I_q, C_q, and G_q are dominated by motion parameters:

$$H_q = \begin{bmatrix}m_f+m_l & 0 & K_1 & K_1\\ 0 & m_f+m_l & K_2 & K_2\\ K_1 & -K_2 & J_f+\frac{1}{3}m_l l_1^2 & \frac{1}{3}m_l l_1^2\\ K_1 & -K_2 & \frac{1}{3}m_l l_1^2 & \frac{1}{3}m_l l_1^2\end{bmatrix} \quad (13a)$$

$$I_q = \begin{bmatrix}0&0&K_2&K_2\\0&0&K_1&K_1\\0&0&0&0\\0&0&0&0\end{bmatrix} \quad (13b)$$

$$C_q = \begin{bmatrix}0&0&0&0&0&2K_2\\0&0&0&0&0&2K_1\\0&0&0&2K_1&2K_1&0\\0&0&0&2K_1&2K_1&0\end{bmatrix} \quad (13c)$$

$$G_q = \begin{bmatrix}(m_f+m_l)g\\0\\K_1\\K_2\end{bmatrix} \quad (13d)$$

$$\begin{cases}K_1 = \frac{1}{2}m_l l\cos(\alpha_{f\leftrightarrow l}+\alpha_f)\\ K_2 = -\frac{1}{2}m_l l\sin(\alpha_{f\leftrightarrow l}+\alpha_f)\end{cases} \quad (13e)$$

If the slides on deformable terrains are ignored and only vertical compaction is executed as illustrated in Fig.3 (b), the Δx, α_{f} will be zero. The final output of normal acceleration is:

$$\begin{aligned}&F_N - G_u\\ &= (m_f+m_l)\Delta\ddot{z} + \frac{1}{2}m_l l\ddot{\alpha}_{f\leftrightarrow l}\cos\alpha_{f\leftrightarrow l} -\\ &\quad \Rightarrow \frac{1}{2}m_l l\dot{\alpha}_{f\leftrightarrow l}^2\sin\alpha_{f\leftrightarrow l} + (m_f+m_l)g \quad (14a)\\ &\Delta\ddot{z}\\ &= \frac{[F_N - G_u + \frac{1}{2}m_l l(\dot{\alpha}_{f\leftrightarrow l}^2\sin\alpha_{f\leftrightarrow l} - \ddot{\alpha}_{f\leftrightarrow l}\cos\alpha_{f\leftrightarrow l})]}{m_f+m_l} - g \quad (14b)\end{aligned}$$

Substituting Eqn. (14a) into the Eqn. (15), the driving torque exerted on the ankle joint based on inverse dynamics while ignoring the tangential force and displacement can be achieved.

$$M = \frac{1}{2}m_l l\Delta\ddot{z}\cos\alpha_{f\leftrightarrow l} + \frac{1}{3}m_l l_1^2\ddot{\alpha}_{f\leftrightarrow l} - \frac{1}{2}m_l l\sin\alpha_{f\leftrightarrow l} \quad (15)$$

Here, the function of F_{N} in Eqn. (15) is expressed by the Fourier function in Eqn. (2). Hence, we set the included angle $\alpha_{\mathrm{f}\leftrightarrow 1}$ within the range of 60° ∼ 135° based on observation of several experiments. We suggest that the ankle rotates at a constant angular velocity, indicating the acceleration of angular velocity is zero. The mass and dimensions of the lower leg and foot have been listed in Table 2. Thus, the ankle torque can be achieved through these information variables: mass of the leg m_l, its length l, the deformation Δz from Eqn. (9), and the angle $\alpha_{\mathrm{f}\leftrightarrow 1}$.

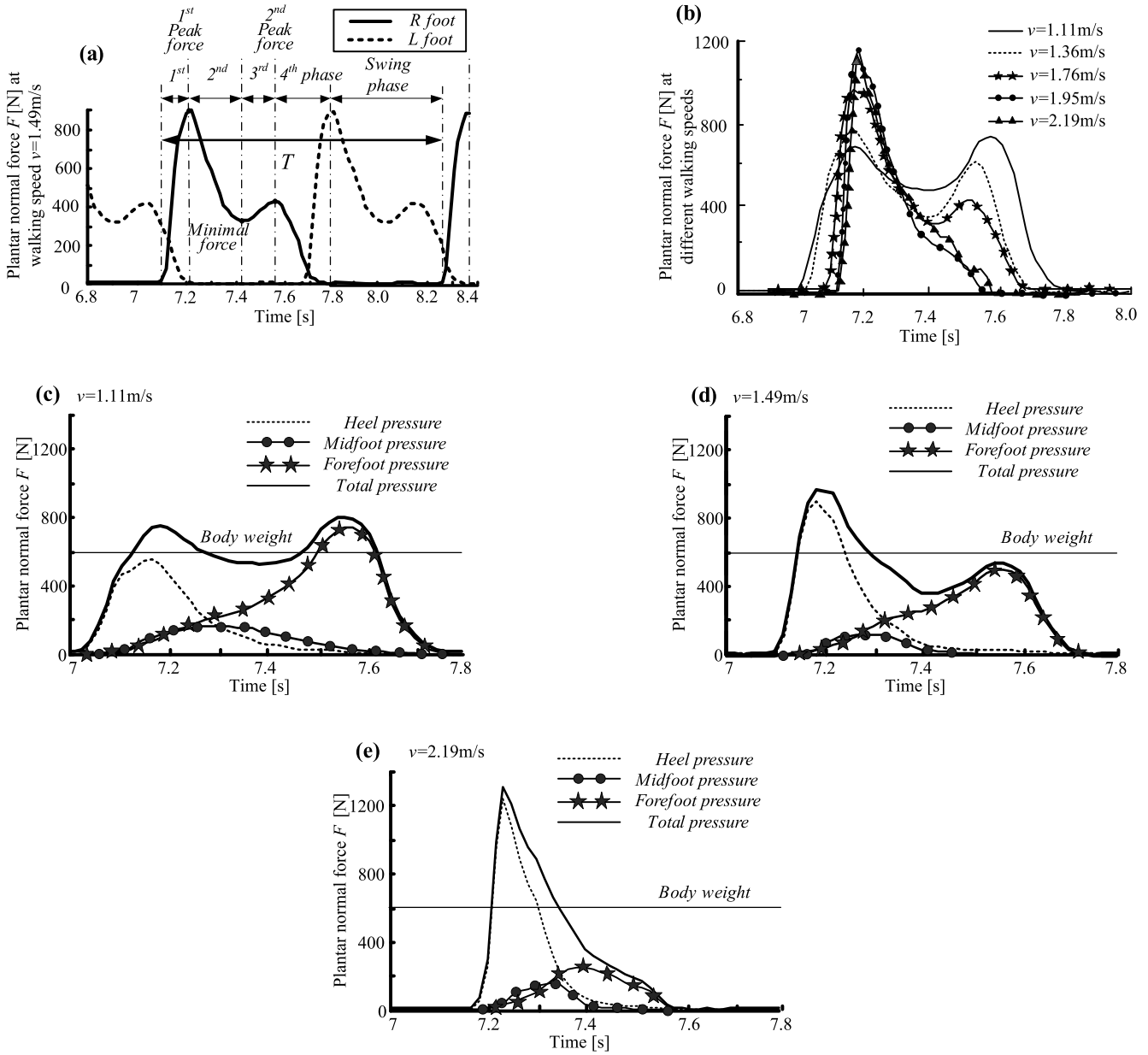

FIGURE 4. Plantar force versus time (a) at conventional speed of 1.49 m/s for experimental subject including the right (R) and left (L) feet, which are indicated by the blue solid and dotted lines respectively; (b) at five walking speeds including 1.11, 1.36, 1.76, 1.95, 2.19m/s during one cycle under the monopod, which are represented by the black solid line, black dotted line, pentacle dotted line, circular dotted line, and triangular dotted line, respectively; of different subsections at three walking speeds including (c) 1.11m/s, (d) 1.49m/s, and (e) 2.19m/s during the same time integral 7s∼7.8s. The dotted line, circular dotted line, and pentacle dotted line indicate the heel, midfoot, and forefoot pressures respectively.

III. RESULTS AND DISCUSSION

A. EXPERIMENTAL RESULTS ON RIGID TERRAIN

Figure 4(a) has illustrated the plantar normal force to contact time at an average walking speed of 1.49 m/s. Four monotonic intervals (called the 1st, 2nd, 3rd, and 4th contact phases from the moment when the heel began to contact with the terrain to that when the forefoot departed from the terrain) are observed during each cycle. The 1st and 3rd are rising phases while the other two decline. Two peak forces and one minimal are observed between these phases. The 1st peak force of the right foot (abbreviated as R foot) appears at the moment when the plantar normal force under the left foot (L foot) just disappeared, and vice versa. The plantar forces under left and right feet are approximately symmetric as observed in color figure output with a time delay in force-time relations. Hence, the time when the single support phase (defined as the period when there is a contact force at only one plantar area, abbreviated to SSP) traverses to the double support phase (DSP) or reverse has been labeled.

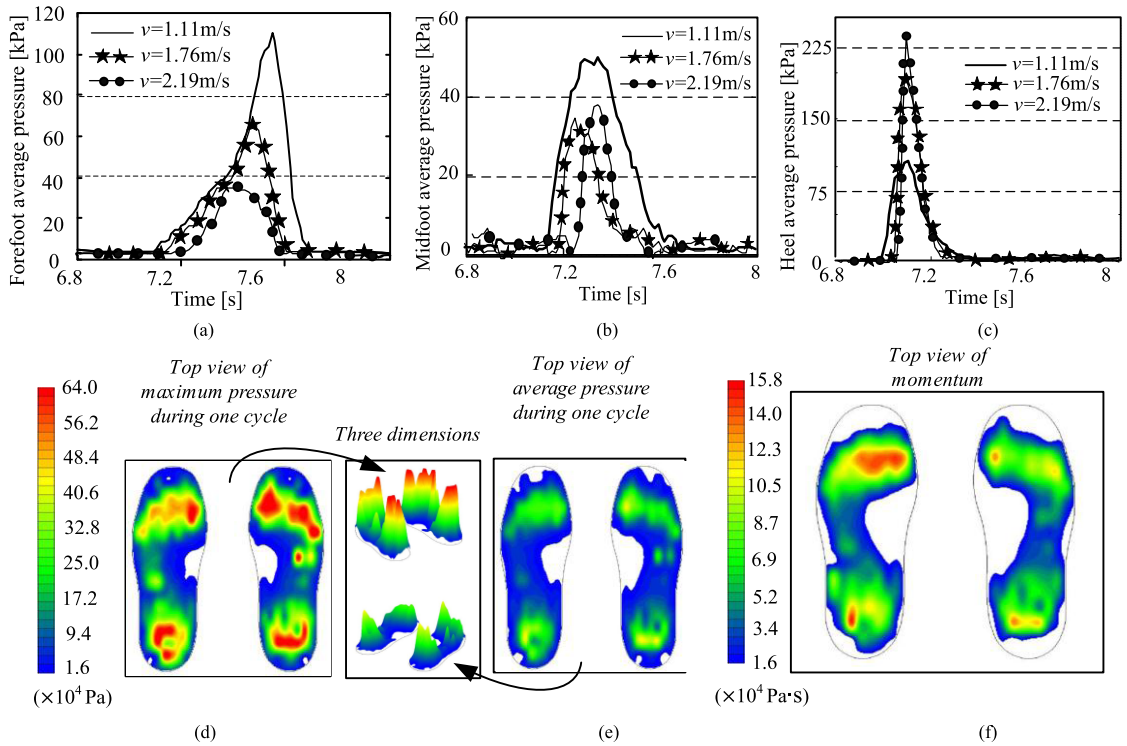

FIGURE 5. Plantar average pressures at three subsections: (a) forefoot, (b) midfoot, and (c) heel; the scales of the time are arbitrarily chosen to be one representative circle at five typical walking speeds; as well as the color maps of the (d) the maximum, (e) average plantar pressures, and (f) momentum during one swing cycle at regular walking speed 1.49m/s from Medilogic data analysis system.

TABLE 2. Values of the stiffness, damping, and exponents of heel.

Body part	*Length (mm)*	*Mass (kg)*	*Moment of inertia (kg·mm²)*
Forefoot	/	0.163	150
Midfoot and heels	/	1.016	3080
Lower leg	358	2.763	35900
Upper body	/	56.86	/

Fig.4 (b) has illustrated the experimental results of the plantar forces versus the contact time at five groups of walking speeds ranging from 1.11 to 2.19m/s. The plantar force-time relations are bimodal functions (with two extreme values) when the speed ranges from 1.11 to 1.75m/s; however, they turned the unimodal (with only one extreme value) functions when the walking is accelerated to the speed range that larger than 1.95m/s. The critical speed, represented by v_b, is estimated to be a magnitude at the speed interval of 1.75∼1.95m/s. With the increasing of speed, the 1st peak force is enlarged, while the 2nd peak and minimal forces is decreased. When walking at a speed that over the v_b, the second peak and minimal points have disappeared. The contact period denoted by Δt (characterized by the time interval when $F > 0$) is enlarged if the walking process slows down, with the following experimental data: $\Delta t_{v=1.11} = 0.83$s, $\Delta t_{v=1.49} = 0.63$s, $\Delta t_{v=2.19} = 0.37$s. Their relations are about $\Delta t_{v=1.11} \approx 1.32\Delta t_{v=1.49} \approx 2.24\Delta t_{v=2.19}$. When the walking speed rises from 1.11m/s to 2.19m/s, the 1st peak pressure has increased for 102% from 572.8N to 1158.7N. When the walking speed rises from 1.11m/s to 1.76m/s, the 2nd peak pressure has declined about 53% from 592.8N to 280.7N; the minimal value has dropped 31% times from 348.6N to 239.5N.

Fig.4 (c∼e) show the experimental results of the heel, midfoot, forefoot pressures at identical time intervals. The waves of heel, midfoot, and forefoot are all unimodal functions in spite of speed ranges. When the moving speed is less than the critical speed v_b (a value at the interval of 1.75∼1.95m/s) such as the occasion of $v = 1.49$m/s, the 1st and 2nd peak values in total pressure are nearly occupied by the maximum values of heel and forefoot pressures, respectively. Furthermore, the time when maximum forefoot force occurred will be advanced in response to accelerations. Though only three speed conditions have been sketched in figures, these principles are considerably derived from overall speed ranges. The magnitude of body weight would be exceeded by the forefoot force at low speed, and the heel force at regular or high speed.

The plantar pressures at three subsections are also illustrated in Fig.5 (a)∼(c). The curves for these normal average pressures are approximately unimodal functions with some fluctuations. The periods of swing cycles will be decreased from 1.233s to 0.783s as the walking speed rises from 1.11m/s

to 2.19m/s. The peak normal stresses for the forefoot are exactly decreased with the augmented speed, while those for the heel are increased. The peak pressures between the heel and rigid terrain remained to be constant if walking at the speed of critical value (1.95m/s) or faster than it. For midfoot, the contact pressure is larger when walking at low speed than that at regular or fast paces. These peak pressures generated by forefoot, midfoot, heel are approximately 116.81kPa, 57.85kPa, and 236.17kPa, respectively. Hence, they will be decreased for 69.16% (forefoot), 21.38% (midfoot) and increased for 105.93% (heel). Concerning on the maximum, average pressures, and their corresponding momentum that in action on plantar areas, we illustrated the experimental color maps in Fig.5 (d)∼(f). From figures, the primary area undergoing pressures for the forefoot seems like a fan-shaped webbed structure; can be regarded as a slender but thick structure like the midsection of the dumbbell; and the heel is a compressed ball. The maximum plantar local pressure will be as large as 640kPa and the maximum momentum generated by the local pressure is about 158kPa.s.

B. EXPERIMENTAL RESULTS ON DEFORMABLE TERRAIN

In our experiments, the plantar forces on two other deformable terrain types including the snow and sand have been measured at perceived regular speed. The average depressions generated by the forefoot and heel on snow were about 8.8mm and 15.2mm, of which are larger than that on sand. It has been found that more vibrations were produced in contact forces versus the time and the majority of which mainly occurred at the 2nd and 3rd phases. The force change rates at 1st and 4th phases, as well as two peak forces, minimal force have been illustrated in Fig.6. The force change rate at phase 1 and phase 4 became small with the increasing depression. Force change rate at 1st phase on hard ground was the largest with the value of 4513 N/s, while the smallest value of 2773 N/s happened on snow as a consequence of buffering effect of compliance terrain. Similarly, it had the largest magnitude of 4705 N/s at the 4th phase when walking on the hard ground and the smallest value of 2314 N/s on the snow. However, the 1st peak force on hard terrain is the smallest (573N) compared to that on snow (636N) and sand (589N). The gaps of 2nd peak values (about 580N) on these three terrain types are not obvious, but the 2nd peak value is tiny smaller when walking on sand due to its flowable property during toe-off phase. For the valley value, it was relatively small on hard ground, but as same magnitude on sand as that on snow. When walking on hard ground, the midfoot was hardly to touch the ground. But on soft terrains like sand and snow, the midfoot would be supported by soft soil particles which perform fluidity. More practical values have been obtained through the experiments, the minimal value on hard ground (349N) is significantly smaller than that on sand and snow (both of them are about 580N), which reveals larger shocks were produced at minimal value on hard terrain. In general, the force change rate will be decreased

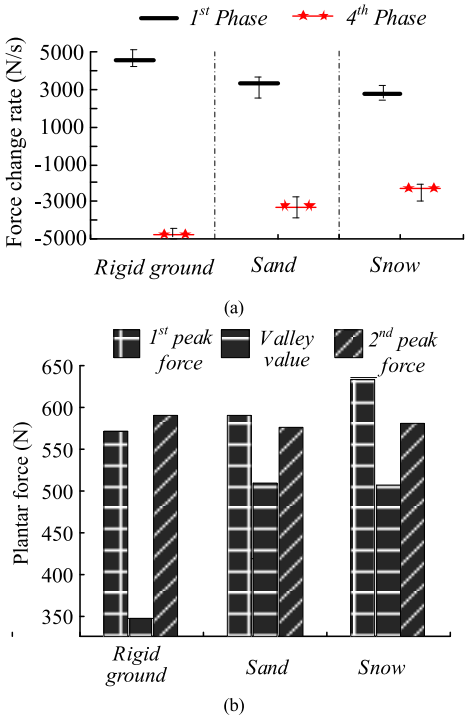

FIGURE 6. Comparison of the 5 parameters: (a) the force change rates at phase 1 and 4; (b) three extreme values among different terrain types including hard ground, sand and snow.

TABLE 3. Fourier parameters at walking speed of 1.49m/s.

Fourier coefficients	$F_{sub1}(t)$	$F_{sub2}(t)$	$F_{sub3}(t)$	$F_{sub1}(t+T_{s\leftrightarrow d})$	$F_{sub2}(t+T_{s\leftrightarrow d})$	$F_{sub3}(t+T_{s\leftrightarrow d})$
ω	7.597	7.66	7.2	7.597	7.66	7.2
a_0	195.4	38.39	137.3	195.4	38.39	137.3
a_1	-38.78	-45.42	52	-163.4	5.987	-180.6
a_2	-71.15	23.78	-159.5	79.34	-28.43	20.67
a_3	-78.98	-10.82	-38.27	-63.12	-14.82	69.84
a_4	-8.34	3.926	66.28	22.96	0.892	-69.36
b_1	-237.6	-25.67	-219.4	176.8	51.83	135.1
b_2	-64.02	22.2	-49.91	-53.54	15.82	-165.8
b_3	22.2	-14.57	102	52.4	-10.46	83.67
b_4	33.22	6.981	20.79	-25.42	-7.959	3.798

with the increase of depression on terrains. The force change rate at phase 1 and 4 decreased 1212.19 N/s and 1450.01 N/s from hard ground to sand, respectively. However, the force change rate of phases 1 and 4 only decreased 528.75 N/s and 941.18 N/ s from sand to snow. Even the depression increased 5.18 times, but the value was only 43.62% and 64.91% of the former due that a solid foundation will inevitably prevented the depression from being extended. As for peak value 1 and peak value 2, their variations with the changing depression were not salient.

The Fourier fitting coefficients are presented in Table 3. Depending on upper fitting functions, we observed that the 1st peak value and phase in total force are primarily caused by the heel-strike, while the 4th phase and 2nd peak value are mainly by toe-off. The rests are generated by three subsections.

TABLE 4. Numerical values of the square of correlation coefficients.

Correlation coefficients	R_1	R_2	R_3	R_4
Numerical values	0.8978	0.7996	0.4719	0.5381
Correlation coefficients	R_5	R_6	R_7	
Numerical values	0.9215	0.5135	0.7110	

During the double support phase (DSP), the majority of plantar force under the lifted foot is taken over by the other lowered foot. The 1st peak force for downward impacting foot occurred at the moment when the uplifting plantar force has just disappeared. At single support phase (SSP), a force transition process from heel to forefoot can be clearly observed from color figures for human feet.

Based on fitting results of R_i, as listed in Table 4, the previous conclusion [9] that there is a linear relationship between walking speed and peak pressures at the heel was proved.

As the average speed v rises from 1.49m/s, perceived regular walking speed, to 2.19m/s, as fast as the experimental subject could achieve, the force change rate of the heel increased dramatically 5.73 times. The 2nd phase has increased 4.64 times when v spans from 1.49m/s to 1.95m/s (critical speed). However, R_3 R_4, and R_6 have not exceeded 0.7, which reveals a poor linear relations of the moving speed with the force change rates at the 3rd and 4th phases, as well as the minimal value. Such phenomenon can be obviously observed in the midfoot, forefoot pressures master curves. The comparisons between experimental results of these force change rates and fitting line are illustrated in Fig.7.

The rising walking speed has enhanced the heel-strike effect on the ground, but generally led to a reduction on forefoot pressure. As the walking process was accelerated, this transition period was significantly shortened and the rebound effect produced by midfoot arc system are further weakened. Before the critical speed, the maximum forefoot pressure was decreased as the moving speed arises. It minimizes when the walking speed equals to 1.95m/s (critical speed) for the subject. Subsequently, the pressure will recover in small amplitude as the speeds continue to increase, suggesting it is suitable for these humans to walking at critical speed if their phalanges or other parts at forefoot part has damaged. Considering the heel, the maximum heel pressure will be increased as the walking speed rises and remains to be constant after the critical value, suggesting walking at a low pace contributes to the rehabilitation of calcaneus. Compared with these anterior and posterior parts, fewer variations have been produced regarding the maximum midfoot pressure with the changing speed on hard ground.

In bionics, a patagium structure in forefoot design helps to distribute the quasi-static net burden from upper body at the plantar area. Depending on analysis based on the fact that

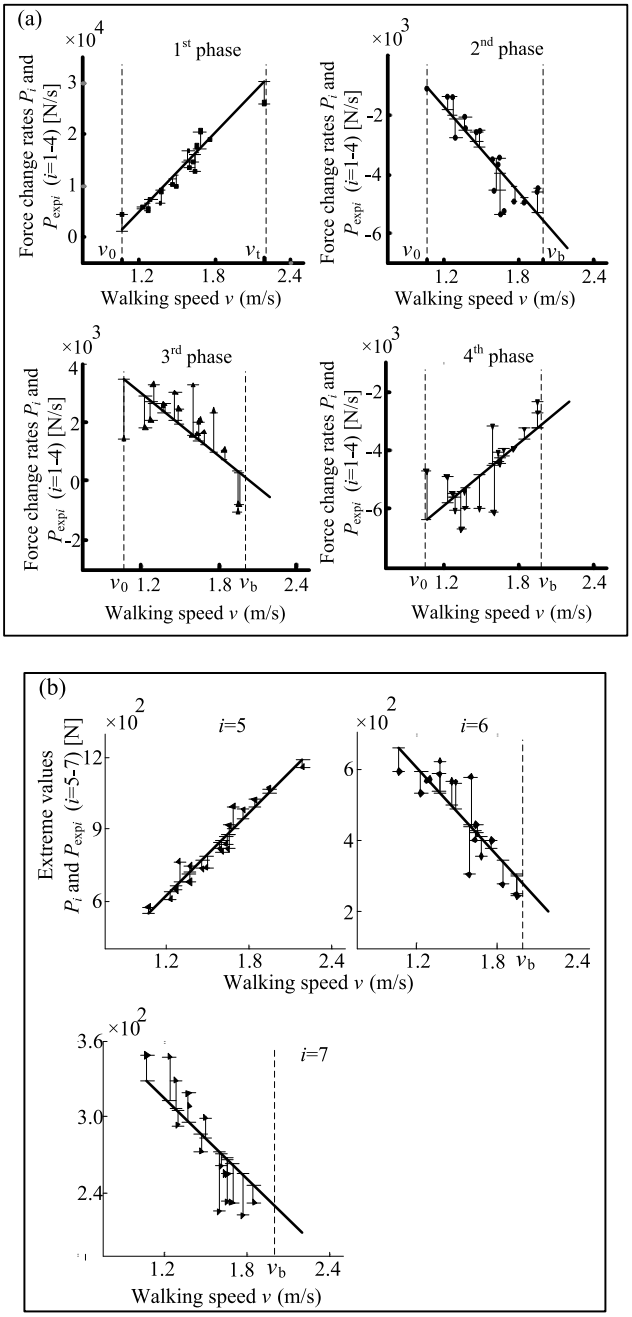

FIGURE 7. Linear fitting functions of the 7 parameters including: (a) The force change rates at four contact phases versus the walking speed v; (b) two peak values (only one peak value is left if walking faster than the critical speed v_b) and one minimal value (vanished when walking at a speed larger than v_b) versus the walking speed. The black points represent the trial data of pressures and the solid line is the theoretical fitting results which have revealed the relations between the parameters and walking speed.

two humps in plantar force-time relations for slow walking and only one remains for fast, heels are better designed to be sphere if a high speed is pursued for biped locomotors on hard ground, since the resistance of such convex structures to impacts is strong, either in dynamics like the basketball and football, or statics like eggs. The arc system in midfoot

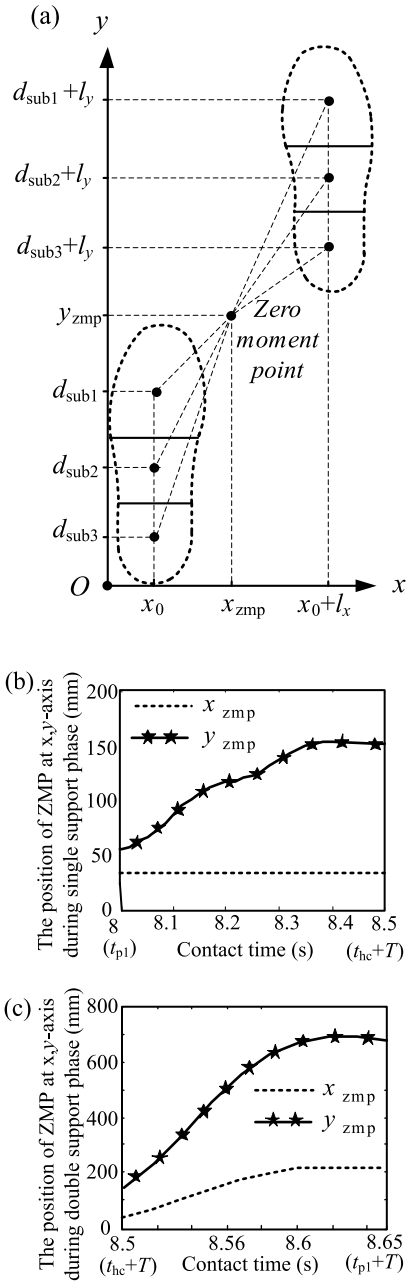

FIGURE 8. Zero moment point positions for biped locomotion when walking speed is 1.49m/s with (a) these constants at fixed speed including the pressure centers of these three subsection at both feet, indicated by the symbols d_{subi}, $d_{subi}+l_y$; numerical simulation results of positions of ZMP calculated with the Eqn. (6) during (b) single support phase and (c) double support phase.

allows feet to save energy and weaken rigid collisions on hard ground.

C. DRIVING ANKLE TORQUE FOR HUMAN IN RIGID CONTACT MODEL

The maximum step length is obtained when the walking speed is about 1.76 m/s. It is concluded that the high speed was triggered by both the increasing frequency and step length, but more heavily on frequency after 1.76m/s. According to

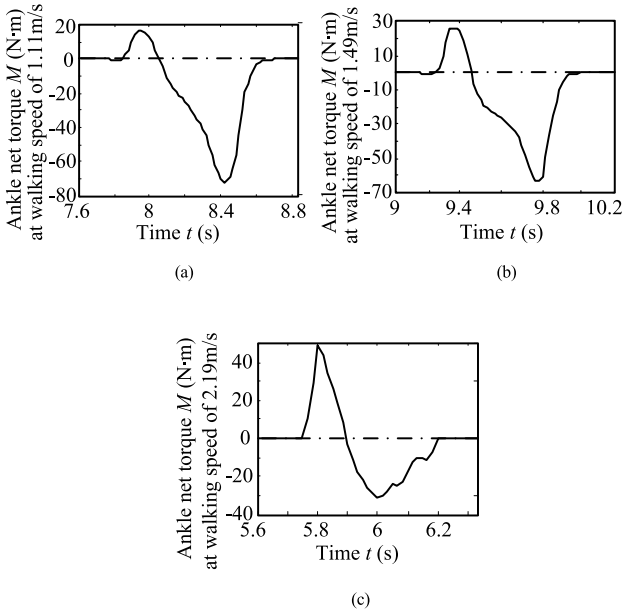

FIGURE 9. Eccentric moments exerted on the ankle when walking at speeds of (a) 1.11m/s, (b) 1.49m/s, and (c) 2.19m/s, respectively. The results were derived from the eqn. (8), with the experimental data of plantar pressures under three subsections.

the energy law, the maximum step length reveals that the center of gravity has reached to the lowest position. Consequently, the least gravitational potential energy, which can be revealed by relative altitude of COM (center of mass), is obtained and the most energy cost is consumed depending on the quasi-static balance when walking at this speed such as 1.76m/s for the subject. Based on experimental results, the variation trend of zero moment point for human are estimated. We conjectured the application points of the heel, midfoot, forefoot pressures were all located on the geometrical centers of these three parts, the times at onset and last of contact process during single and double support phases are chosen to be at one cycle. The step length, indicating the distance along the y direction between the left and right feet, and position of zero moment point, represented by the x and y coordinates, are shown in Fig.8. Here, the trajectories defined as previous section, indicate the dynamically changed horizontal (x direction) and vertical (y direction) coordinates of ZMP (zero moment point) position.

Based on the information of zero moment point and Eqn. (8), the derived driving ankle torque is shown in Fig.9. The lower speed leads to a larger net moment on the ankle joint, while fast paces will enhance the resisting moment at the ankle joint. To maintain the stability and balance of biped walking, an additional inertial moment should be added to resist the eccentric moment about the touch point of zero moment point. Customarily, the left limb is preferably to be swung backward if we kick the left foot forward. We found zero moment point trajectories of biped walking for humans resemble to that for snakes and lizards who wriggle through the sands. Consequently, a senior trajectory plan of zero

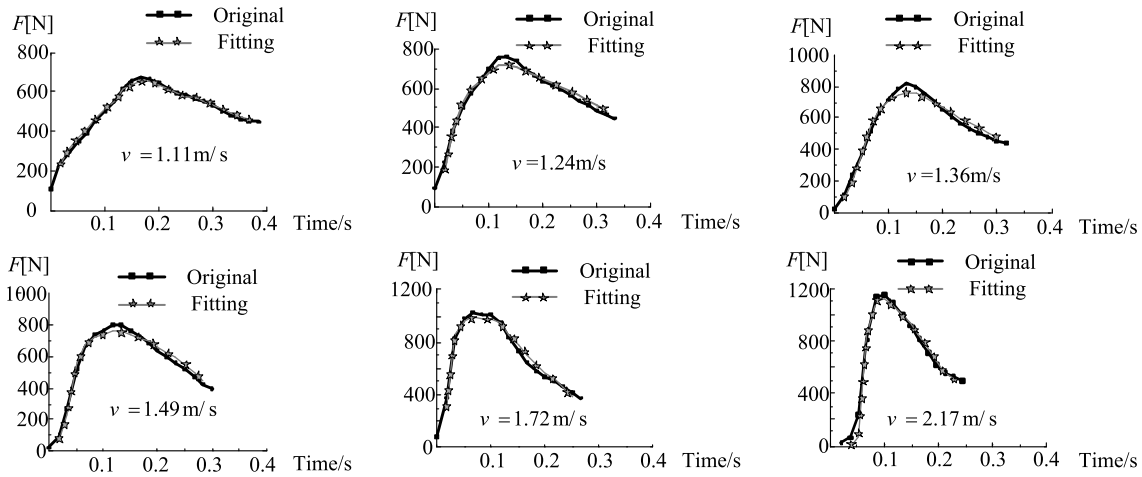

FIGURE 10. Spring-dashpot fitting curves. Comparison of the fitting curve and original data of ground reaction force within heel region under different walking speeds. The astroid is the fitting curve and the line is original data from experimental results. Fitting parameters K, n, C, p, q in foot-ground interaction models have been listed in Table 5.

moment point for biped locomotion can be referred to that for reptiles.

D. DRIVING ANKLE TORQUE FOR HUMAN IN SIMPLIFIED LOWER LIMB-FOOT SYSTEM

Fig.10 has illustrated these fitting curves based on the spring-dashpot model. Moreover, the identified parameters in heel contact model and there are good agreements between fitting curves and experimental data. We found the stiffness was about 10000 N/m with little deviations if the walking speed spanned from 1.11 to 1.63m/s. When acceleration is continued, stiffness K will be increased enormously. For example, the stiffness at walking speeds of 1.72m/s and 2.17m/s are 17342 N/m and 43090 N/m, respectively. One reason is that the increasing walking speed could lead to the contact forces spread from the deforming tissues to calcaneus which performs a higher stiffness. Another can be attributed to the relevance to alteration of vitro or in-situ stress-strain relations used to characterize the plantar soft tissue behavior [21], in which the stiffness and exponential index are about 4006.04kN/m 6.14 and 4.14, respectively. The exponent of stiffness n is generally constant about 3.6. During forefoot contact at 4th phase, we also used the Spring-dashpot model and these parameters, in which damping can be negligibly considered. Hence, the master curves in describing the midfoot interaction can be established using the form of Spring-dashpot model (or Hunt-Crossley model in some literatures) at the 2nd and 3rd phases. All identified stiffness for contact forefoot and midfoot nearly equal 1×104N/mn ($K = 10064, 10010, 10000, 10005, 10000$ at speed of 1.27, 1.37, 1.48, 1.63, 1.76m/s respectively), which is approximately equals to the heel stiffness at regular speed. The magnitudes of parameters n, C, p, q at walking speeds ranging from 1.27 to 1.76m/s have performed similar vibrations around the regular values as heel and forefoot contact models.

TABLE 5. Values of the stiffness, damping, and exponents of heel.

Moving speed v (m/s)	K (N/m^n)	n	C (Ns^q/m^n)	p	q
1.11	10096	3.74	3.79	-6.52	-2.93
1.24	10164	3.62	0.63	-5.16	-0.89
1.36	10306	3.62	2.57	4.07	4.87
1.49	10044	3.55	6.38	11.09	11.56
1.72	17342	3.92	-2.55	46.9	21.22
2.17	43090	5.24	-4.04	15.6	4.43

Other identified parameters of the stiffness, damping, and exponents of the heel have been shown in Table 5.

The parameters for forefoot and midfoot are similar to that for the heel while the walking speed ranges from 1.11 to 1.72. For instance: $K = 10368$N/m^n, $n = 3.58$, $C = 1.79$, $p = -3.24$, and $q = 1.57$ for midfoot when walking at the speed of 1.24m/s. It indicates that the stiffness of forefoot and midfoot are not significantly changed if accelerating the paces. Thus, the identified parameters for forefoot and midfoot are not listed out, which are approximated by that for heels.

Considering the deformable terrains, pressure of peak value 1 and peak value 2 was primarily determined by the walking speed v and supposed even, the body weight of a subject under the same walking patterns. While walking on deformable terrain or even fluidized particles, a sufficient bearing capacity and shearing resistance cannot be supplied by the substrates at the surface supporting the upper body at initial interaction, normal and tangential displacements are both generated at the plantar area. We have found that the detailed stride length was the shortest on sand and longest on rigid ground at perceived regular speeds. As a result, part of mechanical energy in walking human is dissipated as heat loss in soil particles frictional lag or terrain deformations on snow or sand, instead of as the vibrations on rigid terrain. With

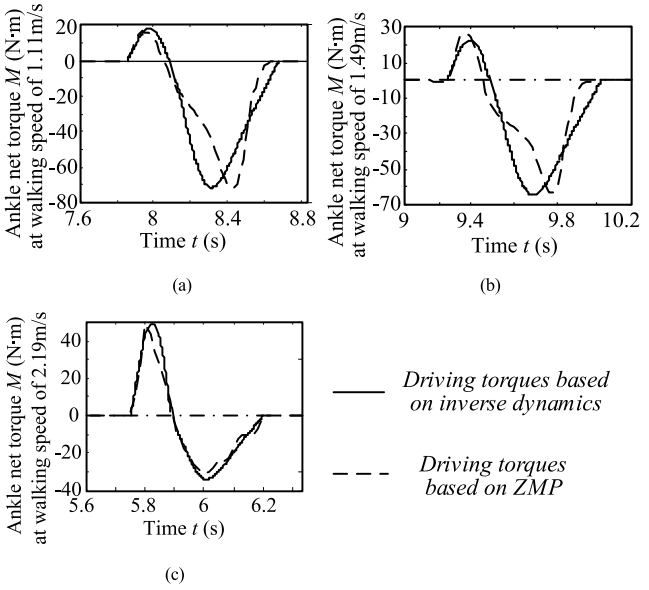

FIGURE 11. Driving torques exerted on the ankle when walking at speeds of (a) 1.11m/s, (b) 1.49m/s, and (c) 2.19m/s, based on Eqns. (8) and (15), with the experimental data of plantar pressures under three subsections.

information of plantar forces, eccentric bending moments, and temporal positions in general coordinate, the control parameters for humanoid robots can be further derived. In the next section, we derived the torque exerted on the ankle joint, as an important and regular design in legged robots.

The Fig.11 shows that the common value of ankle torque is within the range from 15N. m to 70N. m. The magnitudes of peak torques that exerted on the ankle joint derived by Eqn. (15) at three speed conditions, as illustrated in Fig.11, are compared with the prediction results from Eqn. (8), as illustrated in Fig.9. Hence, the relative errors between them are smaller than 10%. Concerning on the biological structure, the human feet composing of the skeleton and soft tissue are constructed as a soft robotic organ in some degree, which indicates that its resisting force may be caused by the creep or stress relaxation, differing from the multi-rigid-chains in deforming principles. For instance, the maximum torque occurs at the moment when the interaction of foot with terrain begins or terminates in multi dynamic models.

With the increasing of walking speed, the 1st peak pressure of F_N, indicated by the parameter P_5 will raise but the 2nd peak pressure denoted by P_7 will decrease. Hence, one single period of a stride cycle will be shortened. According to Eqn. (14a), the magnitude of normal acceleration has a positive correlation with the foot-terrain interaction force F_N ($F_N > 0$). Thus associated with Eqn. (15), the magnitude of ankle torque will be increased and that of resisting torque will be decreased. The upper analysis can be also used to derive the hip joint torque, dominated by passive walking patterns. The faster walking process leads to a more balanced ankle moment, indicating that an equivalent inverted pendulum module can be used in the field of high-speed walking humanoid robot simulations and control, instead of slow walking.

IV. CONCLUSIONS

To conclude, we have experimentally and theoretically studied the interaction mechanics for the human locomotion under three subsections, with its further implications: varying locations of zero moment point, bearing ankle torques, and mechanical properties on deformable terrain.

1) Different amount of humps are demonstrated considering various walking speeds. In particular after filtrations of these experimental data, bimodal functions of force-time relation were observed at low or regular speed, whereas only one peak remains at high speed. The critical speed as the division between single and double peaks was estimated to be 1.95 m/s, which is about 25% larger than the regular speed.

2) The force-time relation at any walking speed can be captured by the summation of that under three isolated morphological contact subsections - the heel, midfoot, and forefoot; accompanied by the accelerating paces, the frequency and stride length are both enlarged with a tuned steps. However, the stride length will be maximized when the speed approaches to the critical value and remains to be steadily and constant after it.

3) Through further derivations, we find the maximum active driving torque undergone by ankles occurred at the critical walking speed. Associated with the greatest stride length, an induction that walking processes at critical speed consume the most considerably energy can be conducted. Moreover, we propose a simplified lower limb-foot mechanism that can be used to investigate the controlled parameters such as the ankle torque for humanoid robot, as well as some common values in design.

4) The impulse generated by the heel stress during single cycle remains to be nearly constant within wide ranges of walking speeds, which implies the contribution by heels to the striking effect within the contact period is unchanged no matter on rigid or deformable terrains. The contact mechanism at heels can be characterized by a superlinear constitutive stress-strain function at initial contact with an additional sublinear during the ending stage; the midfoot plays a more important role in walking on deformable or fluidized terrain surface compared with the rigid ground.

Plantar force-time and deformation relations are two important indexes to evaluate the trafficability of legged robots. Our study has enhanced the understanding of how to change the driving torques if we want to fasten paces, though the feet structures should be considered. A webbed forefoot design is suggested if the robots walk on deformable terrain, while a sphere structure is appropriate in heels design for both rigid and deformable occasions.

REFERENCES

[1] M. Wahde and J. Pettersson, "A brief review of bipedal robotics research," in *Proc. 8th U.K. Mechatron. Forum Int.Conf.*, 2002, pp. 480–488.

[2] M. Kingsbury, "A robophysics approach to bipedal walking in granular media," Ph.D. dissertation, Dept. School Phys., Georgia Inst. Technol., Atlanta, GA, USA, 2016.

[3] A. E. Martin, D. C. Post, and J. P. Schmiedeler, "The effects of foot geometric properties on the gait of planar bipeds walking under HZD-based control," *Int. J. Robot. Res.*, vol. 33, no. 12, pp. 1530–1543, 2014.
[4] F. Abouaesha, C. H. Van Schie, G. D. Griffths, R. J. Young, and A. J. Boulton, "Plantar tissue thickness is related to peak plantar pressure in the high-risk diabetic foot," *Diabetes Care*, vol. 24, no. 7, pp. 1270–1274, 2001.
[5] T. A. Bacarin, I. C. N. Sacco, and E. M. Hennig, "Plantar pressure distribution patterns during gait in diabetic neuropathy patients with a history of foot ulcers," *Clinics*, vol. 64, no. 2, pp. 113–120, 2009.
[6] J. Petrofsky, S. Lee, and S. Bweir, "Gait characteristics in people with type 2 diabetes mellitus," *Eur. J. Appl. Physiol.*, vol. 93, nos. 5–6, pp. 640–647, 2005.
[7] R. J. Griffin, G. Wiedebach, S. Bertrand, A. Leonessa, and J. Pratt, "Walking stabilization using step timing and location adjustment on the humanoid robot, atlas," in *Proc. IEEE/RSJ Int. Conf. Intell. Robots Syst. (IROS)*, Sep. 2017, pp. 667–673.
[8] D. Rosenbaum, S. Hautmann, M. Gold, and L. Claes, "Effects of walking speed on plantar pressure patterns and hindfoot angular motion," *Gait Posture*, vol. 2, pp. 191–197, Sep. 1994.
[9] G. L. Warren, R. M. Maher, and E. J. Higbie, "Temporal patterns of plantar pressures and lower-leg muscle activity during walking: Effect of speed," *Gait Posture*, vol. 19, pp. 91–100, Feb. 2004.
[10] A. Segal, E. Rohr, M. Orendurff, J. Shofer, M. O'Brien, and B. Sangeorzan, "The effect of walking speed on peak plantar pressure," *Foot Ankle Int.*, vol. 25, no. 12, pp. 926–933, 2004.
[11] B. Drerup, U. Hafkemeyer, M. Möller, and H. H. Wetz, "Effect of walking speed on pressure distribution of orthopedic shoe technology," *Orthopade*, vol. 30, no. 3, pp. 169–175, 2001.
[12] P. Rangra, D. Santos, A. Coda, and K. Jagadamma, "The influence of walking speed and heel height on peak plantar pressure in the forefoot of healthy adults: A pilot study," *Clin. Res. Foot Ankle*, vol. 5, no. 2, p. 239, 2017. doi: 10.4172/2329-910X.1000239.
[13] T. W. Dorn, Y.-C. Lin, and M. G. Pandy, "Estimates of muscle function in human gait depend on how foot-ground contact is modelled," *Comput. Methods Biomechanics Biomed. Eng.*, vol. 15, no. 6, pp. 657–668, 2012.
[14] A. Mahboobin, R. Cham, and S. J. Piazza, "The impact of a systematic reduction in shoe–floor friction on heel contact walking kinematics—A gait simulation approach," *J. Biomechanics*, vol. 43, no. 8, pp. 1532–1539, 2010.
[15] G. A. Cavagna, H. Thys, and A. Zamboni, "The sources of external work in level walking and running," *J. Physiol.*, vol. 262, no. 3, pp. 639–657, 1976.
[16] T. R. Han, N. J. Paik, and M. S. Im, "Quantification of the path of center of pressure (COP) using an F-scan in-shoe transducer," *Gait Posture*, vol. 10, no. 3, pp. 248–254, 1999.
[17] B. Van Gheluwe, J. Smekens, and P. Roosen, "Electrodynographic evaluation of the foot during treadmill versus overground locomotion," *J. Amer. Podiatric Med. Assoc.*, vol. 84, no. 12, pp. 598–606, 1994.
[18] T. Warabi, M. Kato, K. Kiriyama, T. Yoshida, and N. Kobayashi, "Treadmill walking and overground walking of human subjects compared by recording sole-floor reaction force," *Neurosci. Res.*, vol. 53, no. 3, pp. 343–348, 2005.
[19] S. Zapolsky and E. Drumwright, "Inverse dynamics with rigid contact and friction," *Auto. Robots*, vol. 41, no. 4, pp. 831–863, 2017.
[20] A. S. Yigit, A. P. Christoforou, and M. A. Majeed, "A nonlinear visco-elastoplastic impact model and the coefficient of restitution," *Nonlinear Dyn.*, vol. 66, no. 4, pp. 509–521, 2011.
[21] K. L. Johnson, "Contact mechanics," Cambridge, U.K.: Cambridge Univ. Press, 1985, pp. 90–106.
[22] V. L. Popov, "Contact mechanics and friction: Physical principles and application," Tech. Rep., 2009.
[23] R. Blickhan, "The spring-mass model for running and hopping," *J. Biomechanics*, vol. 22, nos. 11–12, pp. 1217–1227, 1989.
[24] D. S. Lopes, R. R. Neptune, J. A. Ambrósio, and M. T. Silva, "A superellipsoid-plane model for simulating foot-ground contact during human gait," *Comput. Methods Biomechanics Biomed. Eng.*, vol. 19, no. 9, pp. 954–963, 2016.
[25] M. Peasgood, E. Kubica, and J. McPhee, "Stabilization of a dynamic walking gait simulation," *J. Comput. Nonlinear Dyn*, vol. 2, no. 1, pp. 65–72, 2007.
[26] J. H. Song, "Dynamics simulation for hexapod robot based on modeling of foot-terrain interaction," Ph.D. dissertation, Dept. Master Degree Eng., Harbin Inst. Technol., Heilongjiang Sheng, China, 2012.
[27] J. Y. Wong, *Terramechanics and Off-Road Vehicle Engineering*. Amsterdam, The Netherlands: Elsevier, 2009.
[28] L. Ding *et al.*, "Foot–terrain interaction mechanics for legged robots: Modeling and experimental validation," *Int. J. Robotic Res.*, vol. 32, no. 13, pp. 1585–1606, 2013.
[29] W. R. Ledoux and J. J. Blevins, "The compressive material properties of the plantar soft tissue," *J. Biomechanics*, vol. 40, no. 13, pp. 2975–2981, 2007.
[30] S. Pai and W. R. Ledoux, "The quasi-linear viscoelastic properties of diabetic and non-diabetic plantar soft tissue," *Ann. Biomed. Eng.*, vol. 39, no. 5, pp. 1517–1527, 2011.
[31] P. Aerts, R. F. Ker, D. de Clercq, and D. W. Ilsley, "The effects of isolation on the mechanics of the human heel pad." *J. Anatomy*, vol. 188, no. 2, pp. 417–423, 1996.
[32] R. Naemi, S. Behforootan, P. Chatzistergos, and N. Chockalingam, "Viscoelasticity in foot-ground interaction," in *Viscoelastic and Viscoplastic Materials*. Rijeka, Croatia: InTech, 2016.
[33] M. S. Shourijeh and J. McPhee, "Forward dynamic optimization of human gait simulations: A global parameterization approach," *J. Comput. Nonlinear Dyn.*, vol. 9, no. 3, 2014, Art. no. 031018.
[34] R. R. Neptune, I. C. Wright, and A. J. van den Bogert, "A method for numerical simulation of single limb ground contact events: Application to heel-toe running," *Comput. Methods Biomech. Biomed. Eng.*, vol. 3, no. 4, pp. 321–334, 2000.
[35] Y. Luximon, Y. Cong, A. Luximon, and M. Zhang, "Effects of heel base size, walking speed, and slope angle on center of pressure trajectory and plantar pressure when wearing high-heeled shoes," *Hum. Movement Sci.*, vol. 41, pp. 307–319, 2015.
[36] D. Lemmon, T. Y. Shiang, A. Hashmi, J. S. Ulbrecht, and P. R. Cavanagh, "The effect of insoles in therapeutic footwear—A finite element approach," *J. Biomechanics*, vol. 30, no. 6, pp. 615–620, 1997.
[37] S. J. Kwon and J. Park, "Kinesiology-based robot foot design for human-like walking," *Int. J. Adv. Robotic Syst.*, vol. 9, no. 259, pp. 1–10, 2012.
[38] D. A. Neumann, *Kinesiology of the Musculoskeletal System: Foundations for Rehabilitation*, 2nd ed. Maryland, MD, USA: Mosby, 2009.
[39] W. Kim and S. Voloshin, "Role of plantar fascia in the load bearing capacity of the human foot," *J. Biomechanics*, vol. 28, no. 9, pp. 1025–1033, 1995.
[40] S. Kagami *et al.*, "Measurement and comparison of humanoid H7 walking with human being," *Robot. Auto. Syst.*, vol. 48, pp. 177–187, Oct. 2004.
[41] A. Goswami, "Postural stability of biped robots and the foot-rotation indicator (FRI) point," *Int. J. Robot. Res.*, vol. 18, no. 18, pp. 523–533, 1999.

CHUANXIAO YANG received the B.S. degree in civil engineering from the Ocean University of China, Qingdao, in 2011, and the M.S. degree in mechanical engineering from the Harbin University of Science and Technology, Harbin, China, in 2014, where he is currently pursuing the Ph.D. degree. His current research interests include the modeling of interaction mechanics between legged locomotors and terrain, biomechanical engineering, mechanism design, and the mechanical behavior of legged robots. He once served a Student Member of the IEEE International Conference on Robotics and Biomimetics, in 2016.

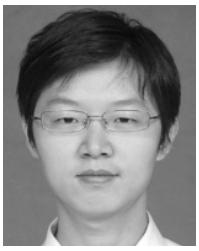

LIANG DING (S'09–M'10–SM'18) was born in Shandong, China, in 1980. He received the Ph.D. degree in mechanical engineering from the Harbin Institute of Technology, Harbin, China, in 2009.

He is currently a Professor and a Doctoral Supervisor with the State Key Laboratory of Robotics and Systems, School of Mechatronics, Harbin Institute of Technology. Since 2009, he has been authoring over 130 articles. He also manages funding projects of the National Natural Science foundation of China for youth and general programs. His research interests include mechanics (terramechanics), control, and simulation for robots and mechatronics systems, in particular, for planetary exploration rovers and multi-legged robots.

Dr. Ding has received the National Second Prize for Technical Invention, in 2011, and the ISTVS Sohne-Hata-Jurecka Award. He has received the Best Paper from the IEEE International Conference on Advanced Robotics and Mechatronics and the paper with best information from the IEEE International Conference on Information and Automation, in 2016. He serves as a Reviewer for several IEEE publications and conferences.

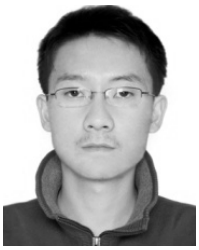

KUNPENG WANG was born in Qinghai, China, in 1993. He received the B.S. and M.S. degrees in mechanical engineering and aerospace engineering from the Harbin Institute of Technology, Harbin, China, in 2016 and 2018, respectively.

He is currently an Engineer in structure design, operation, and debugging of unmanned aerial vehicles. He was involved in establishing the simulations for submarine legged dynamic systems.

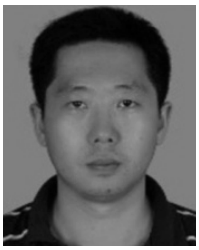

RONG SONG (M'13) received the B.S. degree in electrical engineering from Tsinghua University, Beijing, China, in 1999, the M.S. degree in electronic engineering from Shantou University, Shantou, China, in 2002, and the Ph.D. degree in biomedical engineering from The Hong Kong Polytechnic University, Hong Kong, in 2006.

He is currently a Professor with the School of Biomedical Engineering, Sun Yat-sen University, China. His research interests include musculoskeletal modeling, biomedical signal processing, human motion analysis, and robot-assisted stroke rehabilitation.

DEWEI TANG was born in Heilongjiang, China, in 1966. He received the master's and Ph.D. degrees in mechanical engineering from the Harbin Institute of Technology, Harbin, China, in 1991 and 2000, respectively, where he is currently a Professor and a Doctoral Supervisor with the State Key Laboratory of Robotics and Systems, School of Mechatronics. Since 2010, he has been participating in the Third Phase Project of the Chinese Lunar Exploration. He is mainly involved in two projects including the drilling and sampling on the moon and the near-earth asteroid sample return. His research interests include drilling performance analysis and enhancement in extreme environments, and undisturbed sampling technique.

HAIBO GAO was born in 1970. He received the Ph.D. degree in mechanical engineering from the Harbin Institute of Technology, in 2003, where he is currently a Professor, a Doctoral Supervisor, and the Vice Dean of the School of Mechatronics.

He has presided over 34 national defense 973, military 863, equipment pre-research, and natural science projects. His research interest includes aerospace mechanism and control.

ZONGQUAN DENG was born in 1956.

He is currently a Professor and a Ph.D. Supervisor with the Harbin Institute of Technology, China, where is also the Vice President. He is also an Academician with the Chinese Academy of Engineering. His research interests include special robotics, and aerospace mechanism and control.